PFC/JA-86-42

Free Electron Lasers with Electromagnetic Standing Wave Wigglers

T. M. Tran[a)], B. G. Danly and J. S. Wurtele

Plasma Fusion Center
Massachusetts Institute of Technology
Cambridge, MA 02139

June 1986

Submitted to the *IEEE Journal of Quantum Electronics*

This work was supported by the U.S. Department of Energy Contract No. DE-AC02-78ET51013.

[a)] Permanent address: CRPP, Association Euratom-Confédération Suisse, EPFL, 21, Av. des Bains, CH-1007 Lausanne, Switzerland

Free Electron Lasers with Electromagnetic Standing Wave Wigglers

T. M. Tran*, B. G. Danly and J. S. Wurtele
Plasma Fusion Center
Massachusetts Institute of Technology
Cambridge, Massachusetts 02139

A detailed analysis of the electromagnetic standing wave wiggler for free-electron lasers (FELs) is conducted for both circular and linear wiggler polarizations, following a single-particle approach. After determination of the unperturbed electron orbits in the wiggler field, the single-particle spontaneous emission spectrum and subsequently the gain in the low gain Compton regime (using the Einstein coefficient method) are explicitly calculated. This analysis results in a clear understanding of the resonance conditions and the coupling strength associated to each resonance of this type of FEL. In particular, a striking feature obtained from this investigation is that the electromagnetic standing wave wiggler FEL, under certain circumstances, exhibits a rich harmonic content. This harmonic content is caused by the presence of both the forward and backward wave components of the standing wave wiggler field. In addition, the nonlinear self consitent equations for this type of FEL are also presented, permitting its further investigation by the theoretical techniques and numerical codes developed for conventional FELs.

*Permanent address: CRPP, Association Euratom-Confédération Suisse, EPFL, 21, Av. des Bains, CH-1007 Lausanne, Switzerland

I. INTRODUCTION

In a free-electron laser, the coherent radiation is produced by a periodic transverse acceleration of the relativistic electrons. This acceleration (or "wiggle" motion) is imposed by a transverse periodic magnetostatic field (the "wiggler") in conventional free-electron lasers [1–3]; the frequency of the induced radiation is given by the well known resonance condition [3]

$$\omega_s/c = k_s = \frac{\beta_{||}}{1-\beta_{||}} k_w \simeq \frac{2\gamma^2}{1+a_w^2} k_w, \tag{1}$$

where $k_w = 2\pi/\lambda_w$ is the wiggler wavenumber, $\gamma = (1-\beta_{||}^2-\beta_{\perp}^2)^{-1/2}$ is the relativistic factor and $a_w = eB_w/(k_w mc)$ is the dimensionless vector potential of the wiggler field. Higher odd harmonics of the fundamental frequency given by Eq.(1) can be produced in a planar magnetostatic wiggler [4]. Because the magnetostatic wiggler period λ_w usually cannot be made much smaller than a few cm, the conventional free-electron laser requires a very high voltage electron beam to reach the visible region of the spectrum.

Recently the backward (relative to the electron propagation) traveling wave electromagnetic wiggler has been considered by many authors [5–14]. The resonance condition in this free-electron laser can be expressed as will be shown later

$$\omega_s/c = k_s = k + \frac{\beta_{||}}{1-\beta_{||}}(k+k_{||}) \simeq k + \frac{2\gamma^2}{1+a_w^2}(k+k_{||}), \tag{2}$$

where $k = \omega/c$ is the total wavenumber and $k_{||}$ is the longitudinal wavenumber of the wiggler field or pump wave. For $k_{||} \simeq k$ (free-space mode), the induced radiation frequency for an electromagnetic wiggler is approximately twice that for a magnetostatic wiggler. Since millimeter and sub-millimeter sources based on cyclotron resonance interactions are capable of producing high power (several MW) with high efficiency [15–17], the electromagnetic wiggler appears attractive for very short wavelength free-electron lasers. To increase the pump wave amplitude a_w, (and consequently improve the FEL gain), the wiggler field can be stored in a high Q resonator [14]. In such a standing wave, the resonance condition driven by the backward component of the wiggler field is still given by Eq.(2); in addition, due to the presence of the forward component, a second resonance can take place in the low frequency region and is given by

$$\omega_s/c = k_s = k + \frac{\beta_{||}}{1-\beta_{||}}(k-k_{||}). \tag{3}$$

It should be noted here that the electron axial motion is not uniform ($\beta_{||} \neq$ const.) in the standing wave wiggler. As will be shown later in this article, strong coupling between the electron transverse

motion and the oscillatory longitudinal motion can occur when the dimensionless pump amplitude a_w is not small ($a_w \geq 0.5$), leading to a complicated spectrum of possible resonances. This behavior occurs in the linearly polarized standing wave (LPSW) wiggler as well as in the circularly polarized standing wave (CPSW) wiggler (in the latter case, the resonance spectrum is somewhat less complicated) in contrast with the magnetostatic wiggler and the traveling wave wiggler where only the linearly polarized wiggler exhibits such a multiple resonance spectrum. To our knowledge, the free-electron laser interaction in a standing wave wiggler and in particular, the effects of the forward component of the pump field on the free-electron laser characteristics have not yet been considered. The analysis of these effects constitutes the main purpose of this work.

This paper is organized as follows. The CPSW wiggler and the LPSW wiggler are analyzed in detail in section II and section III respectively. In each case, the electron trajectories in the pump field are derived analytically. Using these trajectories, the spontaneous emission [18] is calculated, from which the resonant frequencies can be deduced. Then the low gain in the Compton regime is derived, using the Einstein coefficient method [19]. The self-consistent equations describing the high gain regime and the nonlinear free-electron laser interaction are presented, as well as a discussion of the power depletion of the pump. Finally, section IV concludes the paper. Throughout this work, the SI units are used.

II. The Circularly Polarized Standing Wave (CPSW) Wiggler

A. *Electron trajectories in the wiggler field*

The CPSW wiggler field is completely defined by the vector potential expressed as follows

$$A_x + iA_y = -\frac{mc}{e}\, a_w \left[e^{i(k_\parallel z + \omega t)} + e^{-i(k_\parallel z - \omega t)} \right], \tag{4}$$

where the pump frequency ω is related to the longitudinal wavenumber $k_\parallel$ by $\omega/c = k = \sqrt{k_\parallel^2 + k_\perp^2}$. The first term and the second term in the rhs of Eq.(4) represent respectively the backward wave and the forward wave of the CPSW field. In open mirror resonators, we can take $k_\perp = 0$ ($k_\parallel = k$); however in practice, a slight misalignment between the electron beam and the resonator axis results in a finite value of $k_\perp$. It is straightforward to show that the pump electric and magnetic fields derived from the vector potential (A_x, A_y) given by Eq.(4) satisfy the boundary conditions at the resonator end walls.

In Eq.(4), we assumed that the wiggler amplitude a_w is independent of the transverse coordi-

nates (x, y), which is accurate if the electron's trajectory is confined near the resonator axis. In this case the electron transverse canonical momenta are constants of motion and assuming ideal injection (zero canonical momentum) yields

$$\gamma\beta_x + i\gamma\beta_y = -a_w \left[e^{i(k_\| z + \omega t)} + e^{-i(k_\| z - \omega t)} \right], \tag{5}$$

and consequently

$$\gamma^2 \beta_\perp^2 = 2a_w^2 (1 + \cos 2k_\| z). \tag{6}$$

The longitudinal equation of motion can be deduced by adopting the canonical momentum $p_\| \equiv \gamma\beta_\|$ as the Hamiltonian with (ct, γ) as the canonical coordinates and z the independent variable [2]

$$h(ct, \gamma; z) \equiv p_\| = \sqrt{\gamma^2 - [1 + 2a_w^2(1 + \cos 2k_\| z)]}. \tag{7}$$

Since the Hamiltonian does not depend on ct, γ is constant ($d\gamma/dz = -\partial h/\partial ct = 0$) and the longitudinal motion is completely determined from the differential equation

$$\frac{d}{dz} ct = \frac{\partial h}{\partial \gamma} = \left[1 - \frac{1 + 2a_w^2(1 + 2\cos 2k_\| z)}{\gamma^2} \right]^{-\frac{1}{2}}. \tag{8}$$

This type of equation can be solved in terms of the elliptic integrals [20]; however, for simplicity we assume that $\gamma \gg 1$ so that Eq.(8) can be approximated by

$$\frac{d}{dz} ct = 1 + \frac{1}{2\gamma^2} \left[1 + 2a_w^2 (1 + \cos 2k_\| z) \right], \tag{9}$$

which can be solved easily. The electron longitudinal motion is then explicitly given by

$$\begin{aligned} ct(z) &= \left(1 + \frac{1 + 2a_w^2}{2\gamma^2} \right) z + \frac{a_w^2}{2\gamma^2} \frac{\sin 2k_\| z}{k_\|} \\ 1/\beta_\|(z) &= 1 + \frac{1 + 2a_w^2}{2\gamma^2} + \frac{a_w^2}{\gamma^2} \cos 2k_\| z. \end{aligned} \tag{10}$$

Note that at cut-off ($k_\| = 0$), the vector potential given by Eq.(4) is similar to a helical magnetostatic wiggler, in which case, the longitudinal motion is uniform [see Eq.(10)]. For nonzero values of $k_\|$, we can define a longitudinal velocity averaged over the pump axial characteristic length $2\pi/k_\|$

$$1/\bar{\beta}_\| = 1 + \frac{1 + 2a_w^2}{2\gamma^2}. \tag{11}$$

Inserting Eq.(10) into Eq.(5) to eliminate the time t, and using the Bessel identity

$$e^{\pm i\delta \sin\theta} = \sum_{n=-\infty}^{\infty} J_{\pm n}(\delta) e^{in\theta}, \tag{12}$$

we obtain

$$\beta_x(z) + i\beta_y(z) = -\frac{a_w}{\gamma} \sum_{n=-\infty}^{\infty} [J_n(\delta) + J_{n+1}(\delta)]\, e^{i\left[k/\bar{\beta}_{\|} + (2n+1)k_{\|}\right]z}, \tag{13}$$

with

$$\delta = \frac{a_w^2}{2\gamma^2} \frac{k}{k_{\|}}.$$

Integrating Eq.(13) in z gives finally the electron orbits in the transverse plane

$$x(z) + iy(z) = i\frac{a_w}{\gamma} \sum_{n=-\infty}^{\infty} [J_n(\delta) + J_{n+1}(\delta)] \frac{e^{i\left[k/\bar{\beta}_{\|} + (2n+1)k_{\|}\right]z} - 1}{k/\bar{\beta}_{\|} + (2n+1)k_{\|}}. \tag{14}$$

From Eq.(13) we can see that the transverse motion in the CPSW wiggler is in general a combination of several harmonic motions, in contrast to the magnetostatic wiggler [21]. The forward wave — and not the electromagnetic nature of the wiggler — is responsible for this behavior as can be deduced from Eqs.(5)–(10) after dropping the forward wave term in Eq.(4). Note that the $n = 0$ term and the $n = -1$ term in the summation can be identified as the respective contributions of the backward wave and the forward wave. For small values of δ, both contributions are equally dominant. With increasing δ, the higher harmonic motions could not be neglected.

Another important feature of the electron dynamics in the CPSW wiggler is that the maximum excursion of the electron (due to the forward wave) away from the axis, deduced from Eq.(14) as

$$|x + iy|_{max} = \frac{a_w}{\gamma} \frac{|J_{-1}(\delta) + J_0(\delta)|}{k/\bar{\beta}_{\|} - k_{\|}}, \tag{15}$$

could be considerable when $k_{\|} \to k$. Thus, the assumption of one-dimensional motion made previously is valid only when

$$\frac{a_w}{\gamma} \frac{k_{\perp}}{k - k_{\|}} \ll 1 \qquad \text{or} \qquad \frac{a_w}{\gamma} \ll \sqrt{\frac{k - k_{\|}}{k + k_{\|}}}. \tag{16}$$

For example, for a $\gamma = 10$ electron beam and a CPSW wiggler having $k_{\|}/k = 0.99$, a_w should be less than 0.71. This treatment would apply to higher values of a_w by decreasing $k_{\|}/k$ and (or) increasing the beam energy γ.

B. Spontaneous emission – Resonance spectrum

By using the method of the Liénard-Wiechert potentials, the spontaneous emission by a single electron undulating close to the wiggler axis can be expressed as [18]

$$\frac{d^2I}{d\Omega d\omega_s} = \frac{e^2\omega_s^2}{16\pi^3\epsilon_o c^3} \left| \int_0^L (\beta_x + i\beta_y) e^{i(k_s z - \omega_s t)} \frac{dz}{\beta_{\|}} \right|^2, \tag{17}$$

where we have introduced (ω_s, k_s) to designate the frequency and the wavenumber of the emitted radiation. The integration of Eq.(17) extends only over the interaction space of length L. In the denominator of the integrand, $\beta_{\|}$ given by Eq.(10) can be approximated by 1. Using the electron trajectory specified by Eqs.(5),(10) and the Bessel relation (12), the integration can be performed in a straightforward manner

$$\frac{d^2I}{d\Omega d\omega_s} = \frac{(ek_sL)^2}{16\pi^3\epsilon_o c}\frac{a_w^2}{\gamma^2}\left|\sum_{n=-\infty}^{\infty} f_n \frac{e^{2i\nu_n}-1}{2i\nu_n}\right|^2, \tag{18}$$

where the coupling coefficient f_n and the resonance parameter ν_n are defined according to

$$f_n \equiv J_{-n}(Q) + J_{-(n+1)}(Q), \qquad Q \equiv \frac{a_w^2}{2\gamma^2}\frac{k_s-k}{k_{\|}}; \tag{19a}$$

$$\nu_n \equiv \frac{L}{2}\left[k + k_{\|} + 2nk_{\|} - (k_s-k)\frac{1+2a_w^2}{2\gamma^2}\right]. \tag{19b}$$

The resonance condition can then be derived as

$$\begin{aligned} &\frac{1+2a_w^2}{2\gamma^2}(k_s-k) = k + k_{\|} + 2nk_{\|}, \\ \text{or} \quad &\frac{1+2a_w^2}{2\gamma^2}k_s = k/\bar{\beta}_{\|} + k_{\|} + 2nk_{\|}, \qquad n = 0, \pm 1, \ldots \end{aligned} \tag{20}$$

where only the values of n such that $k_s = \omega_s/c$ is positive are meaningful. Note that the squared sum in Eq.(18) can be written as

$$\sum_{n=-\infty}^{\infty} f_n^2 \frac{\sin^2\nu_n}{\nu_n^2} + \sum_{n=-\infty}^{\infty}\sum_{m\neq n} C_{m,n},$$

where the cross terms $C_{m,n}$ which can be written as

$$C_{m,n} = \frac{f_n f_m}{4\nu_n\nu_m}\left[1 + \cos 2(\nu_n - \nu_m) - \cos 2\nu_n - \cos 2\nu_m\right]$$

describe the interference between the n^{th} resonance and its neighbouring resonances $n\pm1, n\pm2, \ldots$ They can be neglected when the resonance peaks given by Eq.(20) are well separated, *i.e.* when

$$|\nu_n - \nu_{n\pm1}| > 2\pi \quad \Rightarrow \quad Lk_{\|} > 2\pi. \tag{21}$$

In that case, in evaluating each individual term of the sum, the argument of the Bessel function Q can be approximated by its value at the resonance

$$\begin{aligned} f_n &\simeq J_{-n}(Q_n) + J_{-(n+1)}(Q_n), \\ Q &\simeq Q_n = \frac{a_w^2}{1+2a_w^2}\left(1 + 2n + \frac{k}{k_{\|}}\right). \end{aligned} \tag{22}$$

For very small values of a_w, all the f_n except f_{-1} and f_0 vanish, leading to a double peak spectrum. However, if $k_{||}/k$ is also small, the amplitude of the other peaks ($\sim f_n^2$) starts to increase rapidly with increasing a_w [see Eq.(22)]. Moreover, the $n = 0$ and $n = -1$ main resonance peaks can disappear completely at relatively small values of a_w since f_{-1} and f_0 are zero respectively at $a_w^2 \simeq 1.3k_{||}/(k - 1.7k_{||})$ and $a_w^2 \simeq 3.1k_{||}/(k - 7.2k_{||})$. These features are illustrated in Fig. 1a for $k_{||}/k = 0.1$. Figure 1b shows that the higher n resonances (with frequencies about twice the fundamental) already appear at $a_w \sim 0.5$.

When $k_{||}/k$ increases, the behavior of f_n as a function of a_w is somewhat more regular as shown in Fig. 2. Up to $a_w = 3$ (which is large for the a_w expected for most electromagnetic wigglers [14]), the $n = 0$ peak is still dominant, apart from the low frequency $n = -1$ peak. As $k_{||} \to k$ (with the inequality (16) satisfied so that the one-dimensional assumption is still valid), we have a spectrum of peaks centered at the harmonic frequencies of the $n = 0$ resonant frequency [see Eq.(20)]. We shall see below that the free-electron laser gain is indeed proportional to f_n^2. Therefore, as far as high radiation frequency generation or amplification is concerned, it is noteworthy that a CPSW wiggler with a large $k_{||}$ is more advantageous than a CPSW wiggler with a small $k_{||}$.

C. Free-electron laser gain

One way to obtain the free-electron gain in the approximation of low gain ($G < 1$) is to employ the Einstein coefficient method which states that the gain — relative change of the radiation power $G = [P(z = L) - P(z = 0)]/P(z = 0)$ — is related to the spontaneous emission function

$$\eta_\omega = \frac{c}{L} \frac{d^2 I}{d\Omega d\omega_s}, \tag{23}$$

by the following relation [19]

$$G = \frac{4\pi^3 c^2 L}{\hbar \omega_s^3} \int \eta_\omega(\gamma') \left[F(\gamma') - F(\gamma)\right] d\gamma'. \tag{24}$$

In writing Eq.(24), we assumed that the electron distribution F is only a function of γ and normalized according to

$$\int F \, d\gamma = N_e, \tag{25}$$

N_e being the electron beam density. In Eq.(24), γ' and γ designate the electron energy before and after the radiative process; they are related by the energy conservation equation

$$mc^2 (\gamma' - \gamma) = \hbar(\omega_s - \omega). \tag{26}$$

Expanding $F(\gamma)$ about $F(\gamma')$ and going to the classical limit $\hbar \to 0$, Eq.(24) can be written as

$$G = -\frac{4\pi^3 L}{m}\frac{\omega_s - \omega}{\omega_s^3}\int F(\gamma)\frac{\partial \eta_\omega}{\partial \gamma}\, d\gamma, \tag{27}$$

after performing an integration by parts. To proceed, we restrict ourselves to the case of a cold electron beam $F(\gamma) = N_e\delta(\gamma - \gamma_o)$. Then, on inserting the relations (23),(18) and (19b) into Eq.(27), we obtain

$$G = -\frac{\omega_p^2 L^3 a_w^2}{4c^2\gamma^3}\frac{1+2a_w^2}{2\gamma^2}(k_s - k)\left\{\sum_{n=-\infty}^{\infty} f_n^2 \frac{d}{d\nu_n}\frac{\sin^2\nu_n}{\nu_n^2} + \sum_{n=-\infty}^{\infty}\sum_{m\neq n}\bar{C}_{m,n}\right\}, \tag{28}$$

where the cross terms $\bar{C}_{m,n}$ are

$$\bar{C}_{m,n} = \frac{1}{2}\frac{f_n f_m}{\nu_n\nu_m}\left\{\sin 2\nu_n + \sin 2\nu_m - \frac{\nu_n+\nu_m}{2\nu_n\nu_m}\left[1 + \cos 2(\nu_n - \nu_m) - \cos 2\nu_n - \cos 2\nu_m\right]\right\},$$

and $\omega_p = \sqrt{e^2 N_e/m\epsilon_o}$ is the non-relativistic electronic plasma frequency. In deriving the above expression, we assumed that the interaction length L satisfies $L(k + k_{\|} + 2nk_{\|})/2 \gg 1$. Indeed, the interference effects (already discussed in the previous section on spontaneous emission) can be neglected when the inequality (21) is satisfied. In that case, the gain associated with the n^{th} resonance is approximated by

$$G_n = -\frac{\omega_p^2 L^3 a_w^2}{4c^2\gamma^3}(k + k_{\|} + 2nk_{\|}) f_n^2 \frac{d}{d\nu_n}\frac{\sin^2\nu_n}{\nu_n^2}. \tag{29}$$

Note that the same result can be also obtained by applying Madey's theorem [22]. The derivative of $-\sin^2\nu_n/\nu_n^2$ has its maximum value equal to 0.5402 when $\nu_n = 1.303$. Thus, the maximum gain G_n can be expressed in terms of the current intensity I (in Amperes) of the electron beam and its cross section A_b as

$$G_{n,max} = 0.996 \times 10^{-4}\frac{I L^3 a_w^2}{A_b\gamma^3}(k + k_{\|} + 2nk_{\|}) f_n^2. \tag{30}$$

We note that the gain expression for the $n = 0$ resonance coincides with the gain (see Eq. 2.21 of ref.[21]) for the helical magnetostatic wiggler by making the substitutions $a_w^2 f_o^2 \to K^2$ and $k + k_{\|} \to k_u$, K and k_u being the dimensionless rms vector potential and the wavenumber of the magnetostatic undulator. In addition, the CPSW wiggler can amplify more than one frequency provided the pump strength a_w is not too small [see Figs.(1) ,(2)] in contrast to the helical magnetostatic undulator.

D. Self-consistent equations of motion

So far, we have analyzed the small signal regime which requires only the knowledge of the unperturbed orbits of the electrons in the pump field. In this section, we are interested in a more

detailed description of the mechanisms of radiation generation and its nonlinear saturation. To this end, we derive a set of self-consistent equations for the CPSW free-electron laser, following closely the methodology used in refs.[2,4].

We assume that the electron beam is sufficiently tenuous that the collective effects are negligible. Hence, the single particle model employed in section II.A is still valid after adding a radiation field (having the same polarization as that of the wiggler field) given by the following vector potential

$$A_{sx} + iA_{sy} = \frac{mc}{e} a_s \epsilon^{-i(k_s z - \omega_s t + \phi_s)} \tag{31}$$

to the pump field in Eq.(4). The radiation dimensionless amplitude a_s and phase ϕ_s are slowly varying functions of z by virtue of the single frequency assumption. For a highly relativistic electron, the longitudinal motion can now be derived from the dimensionless Hamiltonian

$$h(ct, \gamma; z) \equiv p_{\|} = \gamma - \frac{1}{2\gamma}\left\{1 + 2a_w^2\left[1 + \cos 2k_{\|}z\right] + a_s^2 - 2a_w a_s\left[\cos\psi + \cos(\psi - 2k_{\|}z)\right]\right\}, \tag{32}$$

where we have introduced the phase ψ defined by

$$\psi \equiv (k_s + k_{\|})z - (\omega_s - \omega)t + \phi_s. \tag{33}$$

In Eq.(32), we can drop the term a_s^2 because usually $a_s \ll a_w$. From the canonical equations, we obtain

$$\frac{d\gamma}{dz} = -\frac{\partial h}{\partial ct} = -\frac{k_s - k}{\gamma} a_w a_s \left\{\sin\psi + \sin(\psi - 2k_{\|}z)\right\} \tag{34a}$$

$$\frac{d}{dz}ct = \frac{\partial h}{\partial \gamma} = 1 + \frac{1}{2\gamma^2}\left\{1 + 2a_w^2\left[1 + \cos 2k_{\|}z\right] - 2a_w a_s\left[\cos\psi + \cos(\psi - 2k_{\|}z)\right]\right\}. \tag{34b}$$

The term containing $\psi - 2k_{\|}z$ describes the contribution from the forward wave component of the pump field. The energy equation (34a) suggests that it is more convenient to choose the phase ψ as a dynamical variable instead of the electron transit time ct. Taking the derivative of ψ as defined by Eq.(33) and making use of the second canonical equation yield then

$$\begin{aligned}\frac{d\psi}{dz} = k + k_{\|} - \frac{1 + 2a_w^2}{2\gamma^2}(k_s - k) - \frac{k_s - k}{\gamma^2}a_w^2 \cos 2k_{\|}z \\ + \frac{k_s - k}{\gamma^2} a_w a_s \left[\cos\psi + \cos(\psi - 2k_{\|}z)\right] + \frac{d\phi_s}{dz},\end{aligned} \tag{35}$$

which replaces Eq.(34b). For finite values of $k_{\|}$, ψ can be decomposed in a slow z-variation term and a fast oscillation. This can be seen by inserting the unperturbed electron trajectory obtained in Eq.(10) into Eq.(33)

$$\psi = \theta - \frac{k_s - k}{\gamma^2}\frac{a_w^2}{2k_{\|}} \sin 2k_{\|}z + \phi_s, \tag{36}$$

where the "slow phase" θ is

$$\theta = \left[k + k_{\|} - (k_s - k)\frac{1 + 2a_w^2}{2\gamma^2}\right] z = \left[k_s + k_{\|} - (\omega_s - \omega)\frac{1}{c\bar{\beta}_{\|}}\right] z, \tag{37}$$

the last equality being obtained by using Eq.(11). The expression describing the evolution of the slow phase θ as given by Eq.(37) can be regarded as the lowest order approximation in the limit where $a_s \to 0$. A better estimate in which the effects of finite values of a_s [resulting in the "force bunching" term as opposed to the "inertial bunching" described by Eq.(37)] are included, can be obtained by considering Eq.(36) as a definition for θ and using Eq.(35) to derive the equation for the slow phase. Repeating the same operation on the energy equation (34a) and using the Bessel relation (12) yield the following coupled nonlinear equations

$$\frac{d\gamma}{dz} = -\frac{k_s - k}{\gamma} a_w a_s \sum_{n=-\infty}^{\infty} f_n \sin(\theta + 2nk_{\|}z + \phi_s), \tag{38a}$$

$$\frac{d\theta}{dz} = k + k_{\|} - (k_s - k)\frac{1 + 2a_w^2}{2\gamma^2} + \frac{k_s - k}{\gamma^2} a_w a_s \sum_{n=-\infty}^{\infty} f_n \cos(\theta + 2nk_{\|}z + \phi_s), \tag{38b}$$

where f_n is the coupling coefficient defined in Eq.(19a). With only a few terms retained in the sums (for example $n = 0$ and $n = -1$), the coupled differential equations (38) describe the interaction between the electrons and the single frequency radiation wave in resonance with the $n = 0$ component of the electron wiggle motion: $k + k_{\|} - (k_s - k)(1 + 2a_w^2)/2\gamma^2 \simeq 0$. The generalization of Eq.(38) to an arbitrary resonance is made straightforwardly by the substitution $\theta \to \theta_n \equiv \theta + 2nk_{\|}z$. This yields

$$\frac{d\gamma}{dz} = -\frac{k_s - k}{\gamma} a_w a_s \sum_{n'=-\infty}^{\infty} f_{n'+n} \sin(\theta_n + 2n'k_{\|}z + \phi_s), \tag{39a}$$

$$\frac{d\theta_n}{dz} = \mu_n + \frac{k_s - k}{\gamma^2} a_w a_s \sum_{n'=-\infty}^{\infty} f_{n'+n} \cos(\theta_n + 2n'k_{\|}z + \phi_s), \tag{39b}$$

where we have introduced the detuning parameter μ_n which is related to the dimensionless resonance parameter ν_n [see Eq.(19b)] by

$$\mu_n = \frac{2}{L}\nu_n = k + k_{\|} + 2nk_{\|} - (k_s - k)\frac{1 + 2a_w^2}{2\gamma^2}. \tag{40}$$

In Eqs.(39), the sums contain both the n^{th} resonant term and the non-resonant ($n' \neq n$) contributions. The detuning parameter μ_n can be also expressed in terms of the resonant energy γ_r

as

$$\mu_n = (k + k_\| + 2nk_\|)\left(1 - \frac{\gamma_r^2}{\gamma^2}\right),$$
$$\gamma_r^2 \equiv \frac{1 + 2a_w^2}{2}\frac{k_s - k}{k + k_\| + 2nk_\|}. \tag{41}$$

In terms of the new canonical coordinates [2] $(\theta_n, \delta\gamma)$, where $\delta\gamma = \gamma - \gamma_r$, and assuming that $\delta\gamma \ll \gamma_r$, one can show that the Hamiltonian for the electron dynamics — given originally by the equations of motion (39) — can then be approximated by

$$h_n(\theta_n, \delta\gamma; z) = (k + k_\| + 2nk_\|)\frac{\delta\gamma^2}{\gamma_r} + F(\theta_n, z), \tag{42}$$

which describes the motion of a particle in a non-stationary potential given by

$$F(\theta_n, z) = -\frac{k_s - k}{\gamma_r}\, a_w a_s \left\{ f_n \cos(\theta_n + \phi_s) + \sum_{n' \neq n} f_{n'+n} \cos(\theta_n + 2n' k_\| z + \phi_s) \right\}. \tag{43}$$

The equation of motion following the Hamiltonian (42) can then be written as a second order differential equation

$$\frac{d^2\theta_n}{dz^2} = \frac{d\mu_n}{dz} = -k_{syn}^2 \left\{ \sin(\theta_n + \phi_s) + \sum_{n' \neq n} \frac{f_{n'+n}}{f_n} \sin(\theta_n + 2n' k_\| z + \phi_s) \right\},$$
$$\text{where} \qquad k_{syn} = 2(k + k_\| + 2nk_\|)\sqrt{\frac{|f_n| a_w a_s}{1 + 2a_w^2}}. \tag{44}$$

If $k_\| L \gg 2\pi$,we can drop the term containing the sum in Eq.(43) by taking an appropriate average of F; the (average) motion can then be regarded as an anharmonic oscillation (like a pendulum) in a quasi-stationary potential well, provided the radiation amplitude and phase a_s, ϕ_s change slowly in z. When $k_\| L$ is small, we should retain the terms in the sum with n' such that $|n'| k_\| L \sim 2\pi$; these terms introduce a slow distortion of the stationary potential and might detrap the otherwise trapped particle. This non-stationary effect is the nonlinear analog to the interferences discussed previously in the small signal regime. Assuming that both the change in a_s and its magnitude are infinitesimal (low gain approximation), one can recover the same gain expression as that given in Eq.(28), by solving Eq.(44) using perturbation theory [21]

The equations governing the self-consistent evolution of the radiation amplitude a_s and phase ϕ_s can be obtained in a standard manner [2]; by inserting Eq.(31) in the Maxwell equations and using Eq.(5) to determine the transverse current density, we obtain

$$\frac{d\hat{a}}{dz} = i\frac{\omega_p^2 a_w}{2c^2 k_s} \left\langle \frac{e^{-i\psi} + e^{-i(\psi - 2k_\| z)}}{\gamma} \right\rangle e^{i\phi_s}. \tag{45}$$

where $\hat{a} \equiv a_s \exp(i\phi_s)$ is the complex amplitude of the radiation field, ψ is given by Eq.(33) and $\langle \cdots \rangle$ denotes an ensemble average over the electrons. Using Eq.(36) and the Bessel relation (12) yields finally

$$\frac{d\hat{a}}{dz} = i\frac{\omega_p^2 a_w}{2c^2 k_s} \sum_{n'=-\infty}^{\infty} f_{n'+n} \left\langle \frac{e^{-i(\theta_n + 2n'k_{\|}z)}}{\gamma} \right\rangle . \tag{46}$$

This complex wave equation describes the self-consistent evolution of the radiation field whose frequency satisfies the n^{th} resonance $\mu_n = 0$ [see Eq.(40)]. Together with the pendulum equations (39) or their simplified version Eq.(44), they form the basic equations for the analysis of the Compton CPSW free-electron laser in the one-dimensional single frequency regime. When the resonance is well isolated, we observe that these equations are analogous to those derived for a conventional free-electron laser; therefore, the numerous theoretical results and numerical codes worked out for the latter can be applied with slight modifications to the CPSW free-electron laser.

E. Power balance – Pump depletion

From the energy equation (39a) and the wave equation (46), it is straightforward to derive the following conservation equation

$$\left(1 - \frac{\omega}{\omega_s}\right) k_s^2 a_s^2 + \frac{\omega_p^2}{c^2}\gamma = \text{constant}. \tag{47}$$

In Eq.(47), the term $k_s^2 a_s^2$ is proportional to the radiation energy flux (Poynting vector) and the second is proportional to the electron beam energy density. Denoting the electron beam power and the laser power by P_b and P_L respectively, this relation implies that the changes of P_b and P_L should satisfy the power balance expressed as

$$-\Delta P_b = \Delta P_L - \frac{\omega}{\omega_s}\Delta P_L. \tag{48}$$

The second term in the rhs of Eq.(48) is obviously the pump depletion; in the quantum picture of the FEL process, this pump depletion is caused by the Compton scattering pump photons from the wiggler field into the laser field by the electrons. Using the definition of the resonant energy γ_r, Eq.(41), the depletion of the pump can be expressed as

$$\Delta P_w = -\frac{\omega}{\omega_s}\Delta P_L \simeq -\frac{\Delta P_L}{2\gamma_r^2}\frac{1 + 2a_w^2}{1 + (2n+1)k_{\|}/k}. \tag{49}$$

Note that the relation (49) can also be derived by the law of conservation of the photon number since $n_{laser} \sim P_L/\omega_s$, and $n_{pump} \sim P_w/\omega$. We observe also that ΔP_w is in direct proportion with

the laser power gain and, therefore, is a potentially important saturation mechanism in the high gain regime ($G \geq 1$). Although the power depletion of the pump represents only a small fraction of the laser power gain, since the energy γ_r is large, it should be taken into account (in addition to the ohmic and diffractive losses in the CPSW cavity) in determining the injected power required to obtain a desired a_w, which can be expressed by the following phenomenological relation

$$P_{inj} = \frac{\omega W}{Q} + \frac{\omega}{\omega_s}\Delta P_L, \tag{50}$$

where Q is the quality factor of the cavity and W is the time averaged stored energy of the CPSW [14].

III. The Linearly Polarized Standing Wave (LPSW) Wiggler

A. *Electron trajectories in the wiggler field*

The electron dynamics in the LPSW wiggler is analyzed by using the same technique as that already presented in section II.A. The linearly polarized pump field is specified by the following vector potential

$$A_x = -\frac{1}{2}\frac{mc}{e}a_w\left[e^{i(k_\parallel z+\omega t)} + e^{-i(k_\parallel z-\omega t)}\right] + \text{c.c.} \tag{51}$$

Assuming perfect electron injection into the interaction space, the transverse motion, confined on the (x,z) plane is then determined by

$$\gamma\beta_x = -a_w\left[\cos(k_\parallel z+\omega t) + \cos(k_\parallel z-\omega t)\right], \tag{52}$$

while the longitudinal motion is described by the coupled differential equations

$$\frac{d}{dz}ct = 1 + \frac{1+a_w^2}{2\gamma^2} + \frac{a_w^2}{2\gamma^2}\left[\cos 2k_\parallel z + (1+\cos 2k_\parallel z)\cos 2kct\right], \tag{53a}$$

$$\frac{d}{dz}\gamma = -\frac{ka_w^2}{\gamma}(1+\cos 2k_\parallel z)\sin 2kct. \tag{53b}$$

Note that the dependent variable ct appears in the rhs of the differential equations; consequently, it is not possible to obtain a straightforward explicit solution to Eq.(53). However, assuming that both $\epsilon_1 \equiv (1+a_w^2)/(2\gamma^2)$ and $\epsilon_2 \equiv a_w^2/(2\gamma^2)$ are small, these equations can be solved by the perturbation method. To the second order in both ϵ_1 and ϵ_2, this yields

$$ct(z) = \left(1+\frac{1+a_w^2}{2\gamma^2}\right)z + \\ + \frac{a_w^2}{4\gamma^2}\left\{\frac{\sin 2k_\parallel z}{k_\parallel} + \frac{\sin 2kz}{k} + \frac{1}{2}\left[\frac{\sin 2(k-k_\parallel)z}{k-k_\parallel} + \frac{\sin 2(k+k_\parallel)z}{k+k_\parallel}\right]\right\}, \tag{54a}$$

and

$$1/\beta_{\|}(z) = 1 + \frac{1+a_w^2}{2\gamma^2} + \\ + \frac{a_w^2}{2\gamma^2}\left\{\cos 2k_{\|}z + \cos 2kz + \frac{1}{2}\left[\cos 2(k-k_{\|}z) + \cos 2(k+k_{\|}z)\right]\right\}. \qquad (54b)$$

The longitudinal motion is now a combination of four harmonic oscillations instead of one as has been found in the CPSW. For later reference, note that for values of $k_{\|}/k$ sufficiently far from 0 and 1, the average longitudinal velocity can be expressed as

$$1/\bar{\beta}_{\|} = 1 + \frac{1+a_w^2}{2\gamma^2}. \qquad (55)$$

Inserting Eq.(54a) into Eq.(52) and using again the Bessel relation (12) yield for the transverse velocity

$$\beta_x(z) = -\frac{a_w}{\gamma}\sum_{n=-\infty}^{\infty}\sum_{m=-\infty}^{\infty} b_{n,m}\cos\left(k/\bar{\beta}_{\|} + k_{\|} + 2nk_{\|} + 2mk\right)z, \qquad (56)$$

where

$$b_{n,m} = \sum_{n'=-\infty}^{\infty}\sum_{m'=-\infty}^{\infty}[J_{n+n'-m'}(\delta_1) + J_{n+n'-m'+1}(\delta_1)]J_{m-n'-m'}(\delta_2)J_{n'}(\delta_3)J_{m'}(\delta_4), \qquad (57a)$$

$$\delta_1 = \frac{a_w^2}{4\gamma^2}\frac{k}{k_{\|}}, \qquad \delta_2 = \frac{a_w^2}{4\gamma^2}, \qquad \delta_3 = \frac{a_w^2}{8\gamma^2}\frac{k}{k-k_{\|}}, \qquad \delta_4 = \frac{a_w^2}{8\gamma^2}\frac{k}{k+k_{\|}}. \qquad (57b)$$

In sharp contrast to the magnetostatic undulator in which the electron transverse motion is a simple harmonic oscillation [21], in the LPSW wiggler the electron has a complex transverse motion which can be decomposed into a discrete spectrum of harmonic oscillations labeled by two integer indices (n,m). This feature suggests that the spontaneous emission and consequently the FEL resonances will have a spectrum very rich in structure. When $a_w \to 0$, only the $n = m = 0$ and $n = -1, m = 0$ Fourier components of β_x have non-zero values. It is easily seen from Eq.(56) that the former component describes the motion in the backward wave of the pump and the latter component describes the motion in the forward wave.

Integrating Eq.(56) once more to obtain the electron trajectory $x = x(z)$, one can see that the maximum excursion of the electron away from the z-axis is determined by

$$x_{max} = \frac{a_w}{\gamma}\frac{|b_{-1,0}|}{k/\bar{\beta}_{\|} - k_{\|}}, \qquad (58)$$

which is similar to the expression (15) obtained for the CPSW case; therefore, the same condition Eq.(16) should be satisfied for the validity of the one-dimensional assumption (no transverse inhomogeneities of the pump field) we made in the above calculations.

B. *Spontaneous emission –Resonance spectrum*

Substituting the electron trajectory specified by Eqs.(52), (54) into the spontaneous emission

$$\frac{d^2I}{d\Omega d\omega_s} = \frac{e^2\omega_s^2}{16\pi^3\epsilon_o c^3}\left|\int_0^L \beta_x e^{i(k_s z-\omega_s t)}\,\frac{dz}{\beta_{\|}}\right|^2, \tag{59}$$

and using the Bessel relation (12) yield, after lengthy algebra,

$$\frac{d^2I}{d\Omega d\omega_s} = \frac{(ek_sL)^2}{16\pi^3\epsilon_o c}\frac{a_w^2}{4\gamma^2}\left|\sum_{n=-\infty}^{\infty}\sum_{m=-\infty}^{\infty}\left[f_{n,m}^{-}\frac{e^{2i\nu_{n,m}^{-}}-1}{2i\nu_{n,m}^{-}} + f_{n,m}^{+}\frac{e^{-2i\nu_{n,m}^{+}}-1}{-2i\nu_{n,m}^{+}}\right]\right|^2, \tag{60}$$

where the resonance parameters $\nu_{n,m}^{\mp}$ and the coupling coefficients $f_{n,m}^{\mp}$ are given by

$$\nu_{n,m}^{\mp} = \frac{L}{2}\left[k/\bar{\beta}_{\|} + k_{\|} + 2nk_{\|} + 2mk \mp k_s\frac{1+a_w^2}{2\gamma^2}\right], \tag{61a}$$

$$f_{n,m}^{\mp} = \sum_{n'=-\infty}^{\infty}\sum_{m'=-\infty}^{\infty}\hat{J}_{-(n+n'-m')}(Q^{\mp})J_{-(m-n'-m')}(R^{\mp})J_{-n'}(S^{\mp})J_{-m'}(T^{\mp}), \tag{61b}$$

with

$$Q^{\mp} = \pm\frac{a_w^2}{4\gamma^2}\frac{k_s \mp k}{k_{\|}}, \qquad R^{\mp} = \pm\frac{a_w^2}{4\gamma^2}\frac{k_s \mp k}{k},$$
$$S^{\mp} = \pm\frac{a_w^2}{8\gamma^2}\frac{k_s \mp k}{k-k_{\|}}, \qquad T^{\mp} = \pm\frac{a_w^2}{8\gamma^2}\frac{k_s \mp k}{k+k_{\|}}, \tag{61c}$$

and

$$\hat{J}_p(z) \equiv J_p(z) + J_{p-1}(z). \tag{61d}$$

The Eq.(60) indicates that the spontaneous emission spectrum is a combination of two distinct spectra denoted by $(-)$ and $(+)$; they represent the respective contributions of the two circularly polarized waves (of opposite helicity) that constitute the LPSW pump field as defined by Eq.(51). It can be easily seen from Eq.(61a) that the spectrum of resonant frequencies generated by one of the two helicities (frequencies satisfying *e.g.* $\nu_{n,m}^{-} = 0$) are in exact symmetry about the origin $k_s = 0$ with those generated by the other helicity ($\nu_{n,m}^{+} = 0$). Furthermore, for highly relativistic electrons ($\beta_{\|} \to 1$), the two spectra almost overlap as implied by

$$\nu_{n,m}^{-} \to -\nu_{-n-1,-m-1}^{+}, \tag{62}$$

for any given pair of integers (n, m). This fact permits us to simplify the spontaneous emission given in Eq.(60) into the following form

$$\frac{d^2I}{d\Omega d\omega_s} = \frac{(ek_sL)^2}{16\pi^3\epsilon_o c}\frac{a_w^2}{4\gamma^2}\sum_{n=-\infty}^{\infty}\sum_{m=-\infty}^{\infty} f_{n,m}^2\frac{\sin^2\nu_{n,m}}{\nu_{n,m}^2}, \tag{63}$$

where $\nu_{n,m}$ and $f_{n,m}$ are now approximated by

$$\nu_{n,m} \simeq \frac{L}{2}\left[k/\bar{\beta}_{\|} + k_{\|} + 2nk_{\|} + 2mk - k_s\frac{1+a_w^2}{2\gamma^2}\right], \tag{64a}$$

$$f_{n,m} \simeq \sum_{n'=-\infty}^{\infty}\sum_{m'=-\infty}^{\infty} \hat{J}_{-(n+n'-m')}(Q_{n,m})\hat{J}_{-(m-n'-m')}(R_{n,m})J_{-n'}(S_{n,m})J_{-m'}(T_{n,m}), \tag{64b}$$

with the arguments of the Bessel functions evaluated at the resonance $\nu_{n,m} = 0$

$$\begin{aligned}
Q_{n,m} &= \frac{a_w^2}{2(1+a_w^2)}\left[1 + 2n + (1+2m)\frac{k}{k_{\|}}\right], \\
R_{n,m} &= \frac{a_w^2}{2(1+a_w^2)}\left[1 + 2m + (1+2n)\frac{k_{\|}}{k}\right], \\
S_{n,m} &= \frac{a_w^2}{4(1+a_w^2)}\left[(1+2n)\frac{k_{\|}}{k-k_{\|}} + (1+2m)\frac{k}{k-k_{\|}}\right], \\
T_{n,m} &= \frac{a_w^2}{4(1+a_w^2)}\left[1 + 2n\frac{k_{\|}}{k+k_{\|}} + 2m\frac{k}{k+k_{\|}}\right].
\end{aligned} \tag{65}$$

In Eq.(63), we neglected the cross terms describing the interferences, by assuming that

$$Lk_{\|} > 2\pi \qquad \text{and} \qquad L(k-k_{\|}) > 2\pi, \tag{66}$$

because the minimum spacing between the resonance peaks is $Lk_{\|}$ or $L(k-k_{\|})$ as implied by Eq.(64a). It is easily seen that the indices $n = 0 = m$ label the resonance due mainly to the interaction with the pump backward wave while the forward wave contribution is identified by $n = -1$, $m = 0$.

In view of the lengthy algebra carried out to obtain Eq.(63), an independent check has been done by computing directly the spontaneous emission as defined by Eq.(59) with the trajectory characteristics $\beta_x(z)$, $ct(z)$ given by Eqs.(52),(54). To this end, the integral in Eq.(59) is rearranged into a Fourier integral so that a Fast Fourier Transform algorithm can be used for the numerical integration. Examples of this direct computation are shown in Fig. 3 and Fig. 4 where the spontaneous emission (divided by the square of the frequency ω_s) is plotted versus the (normalized) frequency for $k_{\|}/k = 0.9$, $\gamma = 20$ and $\bar{L} \equiv (k+k_{\|})L/(2\pi) = 50$. Strictly speaking, the quantity $\bar{L}$ can be viewed as the number of wiggler periods *only when considering the* $n = 0 = m$ *resonance.* In Fig. 3, $a_w = 0.1$ and, as expected, the resonance spectrum exhibits only two peaks centered at $\nu_{0,0} = 0$ and $\nu_{-1,0} = 0$ respectively. For $a_w = 1$, Fig. 4 shows a more complex multiple peak spectrum. A close examination reveals that (a) the positions of the peaks are exactly defined by the resonance conditions $\nu_{n,m} = 0$ [see Eq.(64a)], and (b) the amplitude of each peak agrees with

the analytic expression obtained for $f_{n,m}$ as given by Eq.(64b) and plotted in Fig. 5 as functions of a_w for the peaks that are labeled in Fig. 4. In particular, the fundamental peak ($n = 0 = m$) almost disappears, in agreement with the $(0,0)$ curve shown in Fig. 5.

Increasing $k_{||}/k$ up to 0.99, for example, with $\bar{L} = 50$, we would expect the interferences between the resonance peaks to become important because the condition expressed in Eq.(66) is being violated: $(k - k_{||})L \simeq \pi/2$. The spontaneous spectrum obtained from the numerical integration for this case is displayed in Fig. 6 for $a_w = 1$. Indeed, the interferences appear only when a_w is sufficiently large that the amplitudes $f_{n,m}$ with $n \neq 0, -1$ and $m \neq 0$ are significant. For $a_w = 0.1$, for example, (the others parameters remaining the same as those of Fig. 5), the computed spectrum has only two peaks and is similar to that shown in Fig. 3.

C. Free-electron laser interaction in the LPSW wiggler

In this section, the analysis of a FEL utilizing the LPSW wiggler will be presented. In view of the analysis conducted in Sec. II.B–II.E for the CPSW case, the key quantities are the resonance parameters $\nu_{n,m}$ and the coupling coefficients $f_{n,m}$. Therefore, because the methodology is identical to that employed previously in Sec. II.B–II.E, we will give below only the final results, omitting most of the lengthy details of the derivation.

C.1. Free-electron laser gain

Applying the Einstein coefficient method to the spontaneous emission given by Eq.(63) as explained in Sec. II.C, the free-electron laser gain associated with the (n,m) resonance in the low gain Compton regime for a cold electron beam can be expressed as

$$G_{n,m} = -\frac{\omega_p^2 L^3}{4c^2\gamma^3}\frac{a_w^2}{4}(k + k_{||} + 2nk_{||} + 2mk) f_{n,m}^2 \frac{d}{d\nu_{n,m}}\left(\frac{\sin^2\nu_{n,m}}{\nu_{n,m}^2}\right). \tag{67}$$

We recall that the (n,m) resonance is given by the condition $\nu_{n,m} = 0$ with $\nu_{n,m}$ defined by Eq.(64a). The coupling coefficients $f_{n,m}$ are given by Eq.(64b).

C.2. Self-consistent equations of motion

The radiation electromagnetic fields in the LPSW wiggler are specified by the vector potential

$$A_{sx} = \frac{1}{2}\frac{mc}{e} a_s e^{-i(k_s z - \omega_s t + \phi_s)} + \text{c.c.} \tag{68}$$

The electron dynamics in this field combined with the pump field given by Eq.(51) is then described by

$$\frac{d}{dz}\gamma = -\frac{k_s - k}{2\gamma} a_w a_s \sum_{n'=-\infty}^{\infty} \sum_{m'=-\infty}^{\infty} f_{n'+n,m'+m} \sin(\theta_{n,m} + 2n'k_{\|}z + 2m'kz + \phi_s), \tag{69a}$$

$$\frac{d}{dz}\theta_{n,m} = \mu_{n,m} + \frac{k_s - k}{2\gamma^2} a_w a_s \sum_{n'=-\infty}^{\infty} \sum_{m'=-\infty}^{\infty} f_{n'+n,m'+m} \cos(\theta_{n,m} + 2n'k_{\|}z + 2m'kz + \phi_s), \tag{69b}$$

where

$$\mu_{n,m} \equiv \frac{2}{L}\nu_{n,m} = k/\bar{\beta}_{\|} + k_{\|} + 2nk_{\|} + 2mk - k_s \frac{1 + a_w^2}{2\gamma^2}, \tag{70}$$

is the detuning parameter. When the electron energy γ evolves close to the resonant energy

$$\gamma_r = \sqrt{\frac{(1 + a_w^2)k_s}{2(k/\bar{\beta}_{\|} + k_{\|} + 2nk_{\|} + 2mk)}}, \tag{71}$$

the equations (69) can be reduced to the second order pendulum equation

$$\begin{aligned} \frac{d^2}{dz^2}\theta_{n,m} &= \frac{d}{dz}\mu_{n,m} \\ &= -k_{syn}^2 \left\{ \sin(\theta_{n,m} + \phi_s) + \sum_{n' \neq n} \sum_{m' \neq m} \frac{f_{n'+n,m'+m}}{f_{n,m}} \sin(\theta_{n,m} + 2n'k_{\|}z + 2m'kz + \phi_s) \right\}, \end{aligned} \tag{72}$$

$$\text{where} \qquad k_{syn} = 2(k + k_{\|} + 2nk_{\|} + 2mk)\sqrt{\frac{|f_{n,m}|a_w a_s}{2(1 + a_w^2)}}.$$

Finally, the self-consistent radiation field $\hat{a} \equiv a_s \exp(i\phi_s)$ evolves according to

$$\frac{d\hat{a}}{dz} = i\frac{\omega_p^2 a_w}{4c^2 k_s} \sum_{n'=-\infty}^{\infty} \sum_{m'=-\infty}^{\infty} f_{n'+n,m'+m} \left\langle \frac{e^{-i(\theta_{n,m} + 2n'k_{\|}z + 2m'kz)}}{\gamma} \right\rangle. \tag{73}$$

It can be readily verified that Eqs.(72),(73) yield in the low gain Compton regime the same gain expression given in Eq.(67).

C.3. Pump depletion

The depletion of the LPSW pump power can be determined by the law of conservation of the photon number in the interaction space, as noted in Sec. II.E. Then, using the definition of the resonant energy γ_r gives an expression for the pump power depletion which is analoguous to Eq.(49)

$$\Delta P_w = -\frac{\omega}{\omega_s}\Delta P_L \simeq -\frac{\Delta P_L}{2\gamma_r^2} \frac{1 + a_w^2}{1 + (2n + 1)k_{\|}/k + 2m}. \tag{74}$$

IV. CONCLUSION

In the present work, we have derived and analyzed the electron motion in an electromagnetic standing wave pump field in circumstances where the transverse gradient of the pump as well as the collective space charge forces are negligible (1D Compton regime). The circular polarization (CPSW) and the linear polarization (LPSW) were both considered in detail. The electron trajectories were used to calculate the single-particle spontaneous emission from which the basic properties of the FEL resonance spectrum along with the coupling strength associated with each resonance were deduced. A striking feature of the standing wave wiggler is that the spontaneous emission (and consequently the gain) spectrum is very rich in harmonic content, with resonance peaks located at $(1+2a_w^2)k_s/(2\gamma^2) = k/\bar{\beta}_{||}+2nk_{||}$ for the CPSW wiggler, and at $(1+a_w^2)k_s/(2\gamma^2) = k/\bar{\beta}_{||}+2nk_{||}+2mk$ for the LPSW wiggler. As a result, under certain circumstances, deleterious effects of the interference between neighbouring resonances can take place, reducing the FEL gain. This happens, however, only in the very special situations where $k_{||}L < 2\pi$ [or $(k - k_{||})L < 2\pi$ for the LPSW wiggler] and when a_w is not small ($a_w > 0.5$).

Another noteworthy result is the FEL gain behavior at moderate values of the wiggler dimensionless amplitude ($a_w > 0.5$). It was found that under certain conditions (see Fig. 1a, 5a), the gain associated with the fundamental resonance ($n = 0 = m$) not only becomes smaller than the gain at higher harmonics, but can also vanish. This effect might be advantageous for operation of an FEL at higher harmonics. However, as pointed out in Sec. II.A, one should bear in mind that for very large values of a_w, the effects of the transverse inhomogeneities of the pump field are no longer negligible. Furthermore, finite values of the electron beam emittance might introduce another constraint in the high pump regime because the transverse profile of the pump field is such that it has a *defocusing effect* [14] on the electron beam instead of a *focusing effect* (inducing the betatron oscillations) which occurs in a magnetostatic undulator [23,24]. Such non-ideal effects as well as others three-dimensional effects (diffraction, finite electron beam radius, etc...) are beyond the scope of this paper and will be addressed elsewhere.

In addition, the single-particle single-frequency nonlinear self-consistent equations describing the free-electron laser interaction in both the CPSW wiggler [Eqs.(39) and (46)] and the LPSW wiggler [Eqs.(69) and (73)] are derived for an arbitrary resonance. Making use of the conservation law derived from these equations, we obtained then an expression for the depletion of the pump power, which is shown to agree with that obtained from the quantum picture of the Compton

scattering process. These equations form a convenient basis for the extension of this work to include the non-ideal effects discussed above.

In conclusion, the basic characteristics of the electromagnetic standing wave wiggler FEL have been investigated, using the single particle spontaneous emission. The important feature of this analysis is that the effects of the wiggler forward wave can be neglected when the pump amplitude a_w is small ($a_w < 0.5$). As a result, the methods employed for the optimization of the conventional FEL gain [23] can still be applied for the CPSW and LPSW FELs, as has been done in Ref.[14]. For higher values of a_w, a wide range of frequencies (higher than the fundamental resonant frequency) can have appreciable gain when the criteria expressed in Eq.(21) and Eq.(66) (respectively for the CPSW wiggler and the LPSW wiggler) are satisfied in order to avoid the interference due to the forward wave component of the wiggler. This resonant behavior makes the electromagnetic standing wave wiggler an interesting approach to the short wavelength FEL, using very high power microwave sources coupled to a high Q resonator.

ACKNOWLEDGEMENTS

The authors are grateful to R. J. Temkin and G. Johnston for helpful discussions. This work was supported by the Department of Energy, the National Science Foundation, the Air Force Office of Scientific Research and the Office of Naval Research. One of the authors (T.M.T.) would like to acknowledge the support received from the Swiss National Science Foundation.

References

[1] P. Sprangle, R. A. Smith, and V. L. Granatstein. Free electron lasers and stimulated scattering from relativistic electron beams. In K. J. Button, editor, *Infrared and Millimeter Waves, Vol.1*, pages 279–327, Academic, New York, 1979.

[2] N. M. Kroll, P. L. Morton, and M. N. Rosenbluth. FEL with variable parameter wigglers. *IEEE J. Quantum Electron.*, 17:1436–1468, 1981.

[3] T. C. Marshall. *Free-Electron Lasers*. Macmillan Publishing Company, New York, 1985.

[4] W. B. Colson. The nonlinear wave equation for higher harmonics in FEL. *IEEE J. Quantum Electron.*, 17:1417–1427, 1981.

[5] R. H. Pantell, G. Soncini, and E. Puthoff. Stimulated photo-electron scattering. *IEEE J. Quantum Electron.*, 4:905–907, 1979.

[6] L. R. Elias. High power, efficient, tunable (uv through ir) free electron laser using low energy electron beams. *Phys. Rev. Lett.*, 42:977–980, 1979.

[7] V. L. Bratmann, N. S. Ginzburg, and M. I. Petelin. Common properties of free-electron lasers. *Opt. Commun.*, 30:409–412, 1979.

[8] H. R. Hiddleston, S. B. Segall, and G. C. Catella. Gain enhanced free electron laser with an electromagnetic pump field. In *Physics of Quantum Electronics, Vol.9*, pages 849–865, Addison-Wesley, Reading, Mass., 1982.

[9] Y. Carmel, V. L. Granatstein, and A. Gover. Demonstration of two-stage backward-wave-oscillator free-electron laser. *Phys. Rev. Lett.*, 51:566–569, 1983.

[10] S. von Laven, S. B. Segall, and J. F. Ward. A low loss quasioptical cavity for a two stage free electron laser (FEL). In *Free Electron Generators of Coherent Radiation*, pages 244–254, SPIE, 1983.

[11] S. Ruschin, A. Friedman, and A. Gover. The nonlinear interaction between an electron and multimode fields in an electromagnetically pumped free electron laser. *IEEE J. Quantum Electron.*, 20:1079–1085, 1984.

[12] V. L. Bratman, G. G. Denisov, N. S. Ginzburg, A. V. Smorgonsky, S. D. Korovin, S. D. Polevin, V. V. Rostov, and M. I. Yalandin. Stimulated scattering of waves in microwave generators with high-current relativistic electron beams: simulation of two-stage free-electron lasers. *Int. J. Electron.*, 59:247–289, 1985.

[13] J. S. Wurtele, G. Bekefi, B. G. Danly, R. C. Davidson, and R. J. Temkin. Gyrotron electromagnetic wiggler for FEL applications. *Bull. Am. Phys. Soc.*, 30:1540, 1985.

[14] B. G. Danly, G. Bekefi, R. C. Davidson, R. J. Temkin, T. M. Tran, and J. S. Wurtele. Gyrotron powered electromagnetic wigglers for free electron lasers. 1986. Submitted to *IEEE J. of Quantum Electron.*

[15] A. Sh. Fix, V. A. Flyagin, A. L. Gol'denberg, V. I. Khiznyak, S. A. Malygin, Sh. E. Tsimring, and V. E. Zapevalov. The problems in increase in power, efficiency and frequency of gyrotrons for plasma investigations. *Int. J. Electron.*, 57:821–826, 1984.

[16] V. A. Flyagin, A. L. Gol'denberg, and N. S. Nusinovich. Powerful gyrotrons. In K. J. Button, editor, *Infrared and Millimeter Waves, Vol.11*, pages 179–225, Academic, New York, 1984.

[17] K. E. Kreischer, B. G. Danly, H. Saito, J. B. Schutkeker, R. J. Temkin, and T. M. Tran. Prospects for high power gyrotrons. *Plasma Phys. and Controlled Fusion*, 27:1449–1459, 1985.

[18] J. D. Jackson. *Classical Electrodynamics*, page 671. J. Wiley, second edition, 1975.

[19] G. Bekefi. *Radiation Process in Plasmas*, chapter 2. J. Wiley, 1966.

[20] I. S. Gradshteyn and I. M. Ryzhik. *Table of Integrals, Series, and Products.* Academic, New York, 1980.

[21] W. B. Colson, G. Dattoli, and F. Ciocci. Angular-gain spectrum of free-electron lasers. *Phys. Rev. A*, 31:828–842, 1985.

[22] J. M. Madey. Relationship between mean radiated energy, mean squared radiated energy and spontaneous power spectrum in a power series expansion of the equations of motion in a free-electron laser. *Nuovo Cimento*, 50:64–80, 1979.

[23] T. I. Smith and J. M. Madey. Realizable free-electron lasers. *Appl. Phys. B*, 27:195–199, 1982.

[24] E. T. Scharlemann. Wiggle plane focusing in linear wigglers. *J. Appl. Phys.*, 58:2154–2161, 1985.

Figures

Fig. 1. The coupling coefficients f_n versus the CPSW wiggler amplitude a_w, as calculated from Eq.(22) for $k_{||}/k = 0.1$. The numbers shown in the parenthesis denote the dimensionless resonant frequency $(1 + 2a_w^2)(k_s - k)/[2\gamma^2(k + k_{||})]$.

Fig. 2. The coupling coefficients f_n versus the CPSW wiggler amplitude a_w, as calculated from Eq.(22) for $k_{||}/k = 0.9$. The numbers shown in the parenthesis denote the dimensionless resonant frequency $(1 + 2a_w^2)(k_s - k)/[2\gamma^2(k + k_{||})]$.

Fig. 3. The (normalized) spontaneous emission spectrum for a LPSW wiggler (with $a_w = 0.1$ and $k_{||}/k = 0.9$), as obtained from a direct calculation (using an FFT algorithm) of Eq.(59). The peaks are identified by the pair of integers (n, m) [see Eq.(64)]. Only the fundamental peaks $n = 0 = m$ and $n = -1, m = 0$ are present because the wiggler amplitude is small.

Fig. 4. The (normalized) spontaneous emission spectrum for a LPSW wiggler (with $a_w = 1$ and $k_{||}/k = 0.9$), as obtained from a direct calculation (using an FFT algorithm) of Eq.(59). The peaks are identified by the pair of integers (n, m) [see Eq.(64)]. Observe that the $(0,0)$ peak almost disappears.

Fig. 5. The coupling coefficients $f_{n,m}$ versus the LPSW wiggler amplitude a_w, as calculated from the analytical expression, Eq.(64b) for $k_{||}/k = 0.9$. The (absolute) amplitude of the peaks shown in Fig. 3 and Fig. 4 should be compared to the square of $f_{n,m}$ for different (n, m).

Fig. 6. The (normalized) spontaneous emission spectrum for a LPSW wiggler (with $a_w = 1$ and $k_{||}/k = 0.99$), as obtained from a direct calculation (using an FFT algorithm) of Eq.(59). The interference effects are no longer negligible because $(k - k_{||})L \simeq \pi/2$ in this case [see Eq.(66)].

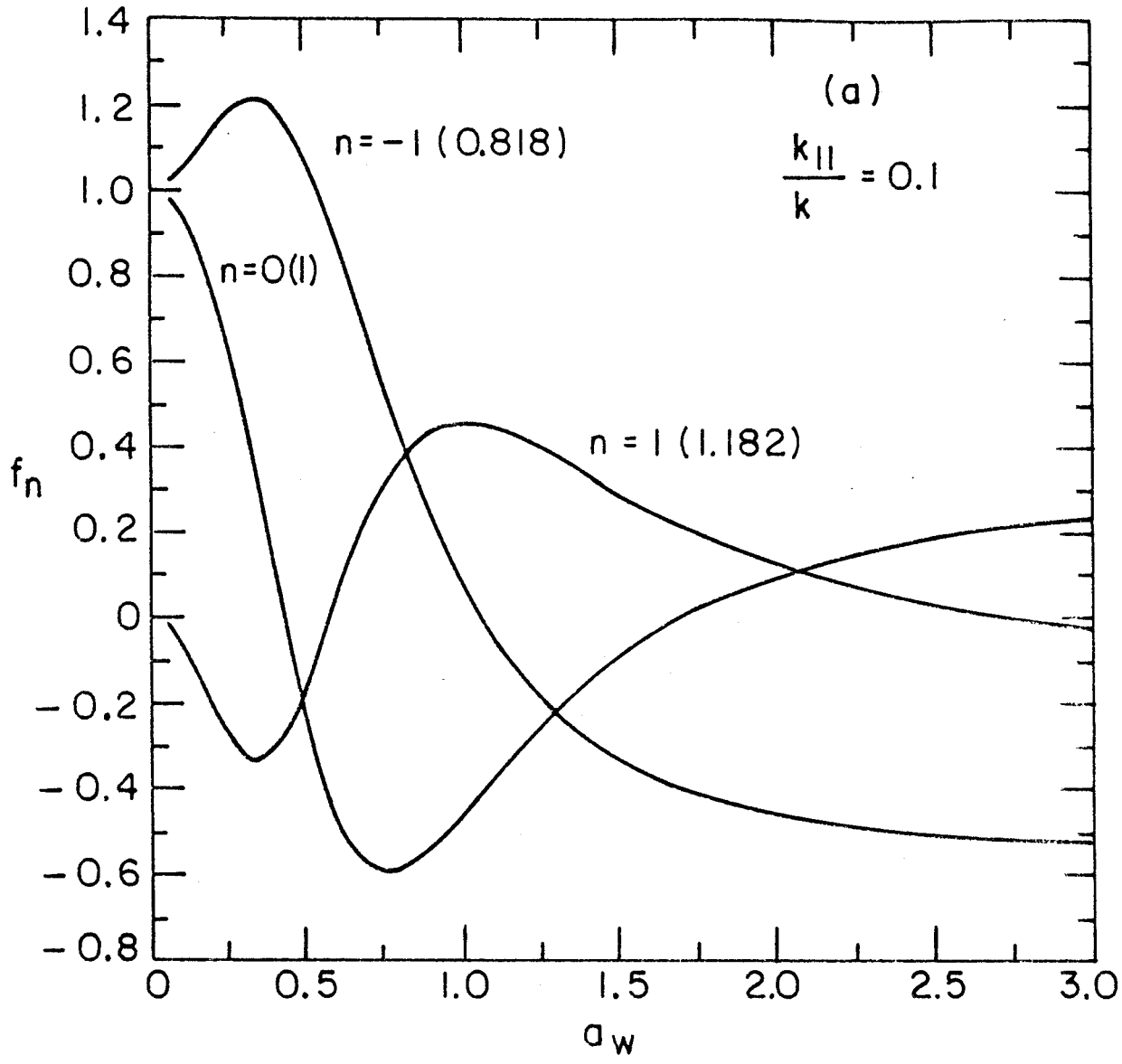
(a)
$\frac{k_{||}}{k} = 0.1$
n = −1 (0.818)
n=0(1)
n = 1 (1.182)
f_n
a_w
1.4
1.2
1.0
0.8
0.6
0.4
0.2
0
−0.2
−0.4
−0.6
−0.8
0
0.5
1.0
1.5
2.0
2.5
3.0

Fig. 1a

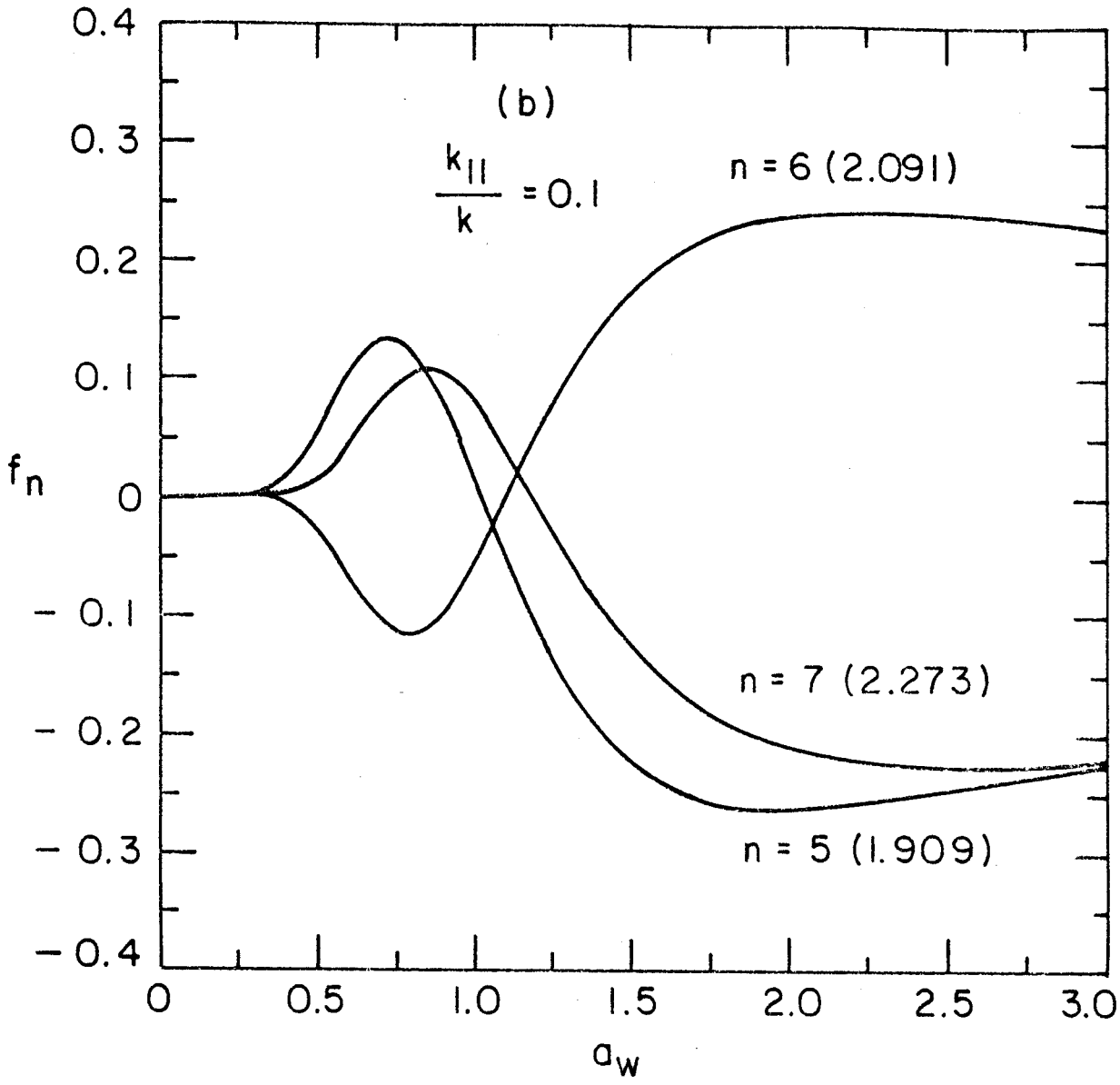
(b)
$\frac{k_{||}}{k}$ = 0.1
n = 6 (2.091)
n = 7 (2.273)
n = 5 (1.909)
f_n
a_w
0.4
0.3
0.2
0.1
0
- 0.1
- 0.2
- 0.3
- 0.4
0
0.5
1.0
1.5
2.0
2.5
3.0

Fig. 1b

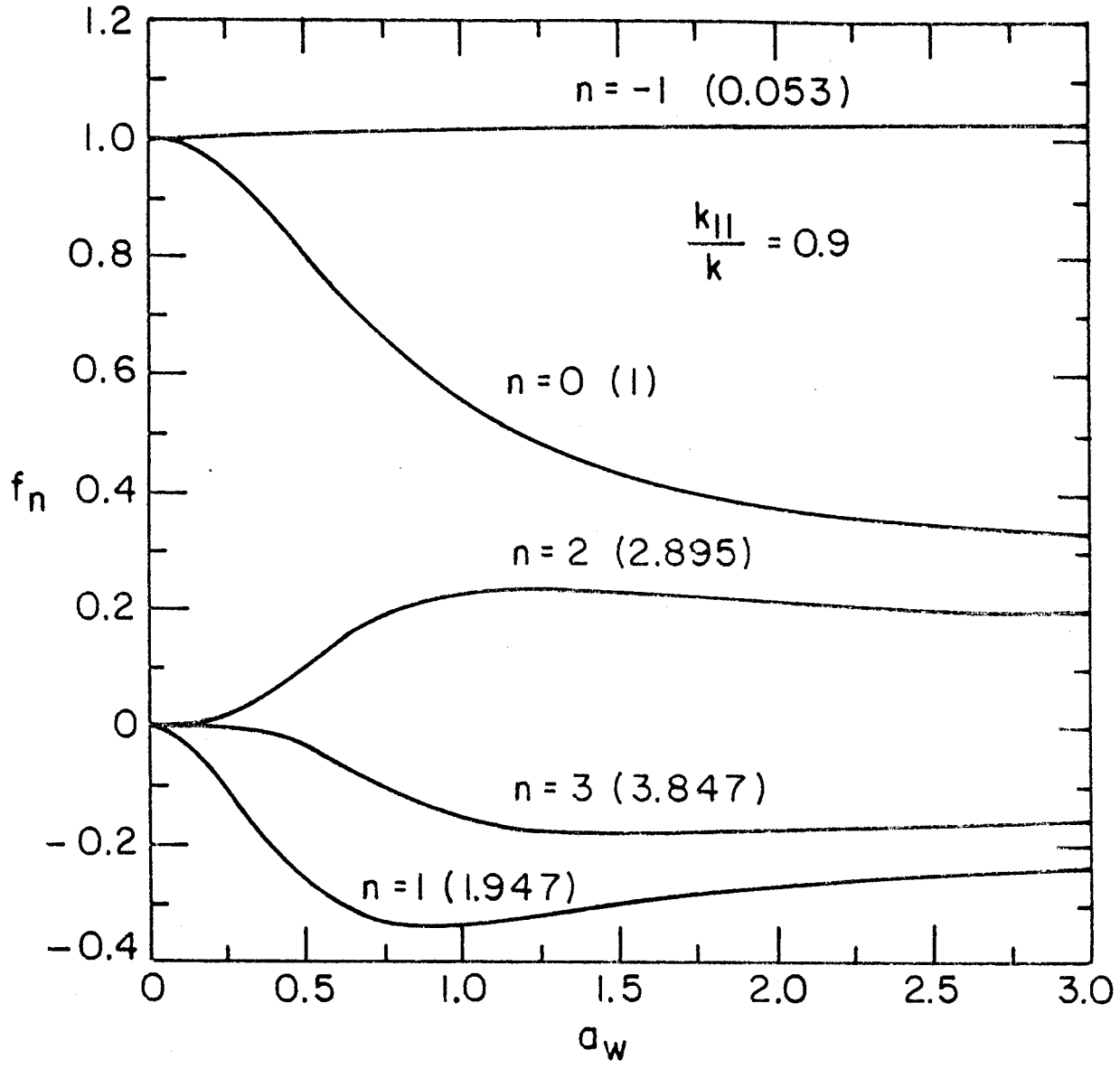
1.2
1.0
0.8
0.6
0.4
0.2
0
-0.2
-0.4
f_n
n = -1 (0.053)
$\frac{k_{||}}{k}$ = 0.9
n = 0 (1)
n = 2 (2.895)
n = 3 (3.847)
n = 1 (1.947)
0
0.5
1.0
1.5
2.0
2.5
3.0
a_w

Fig. 2

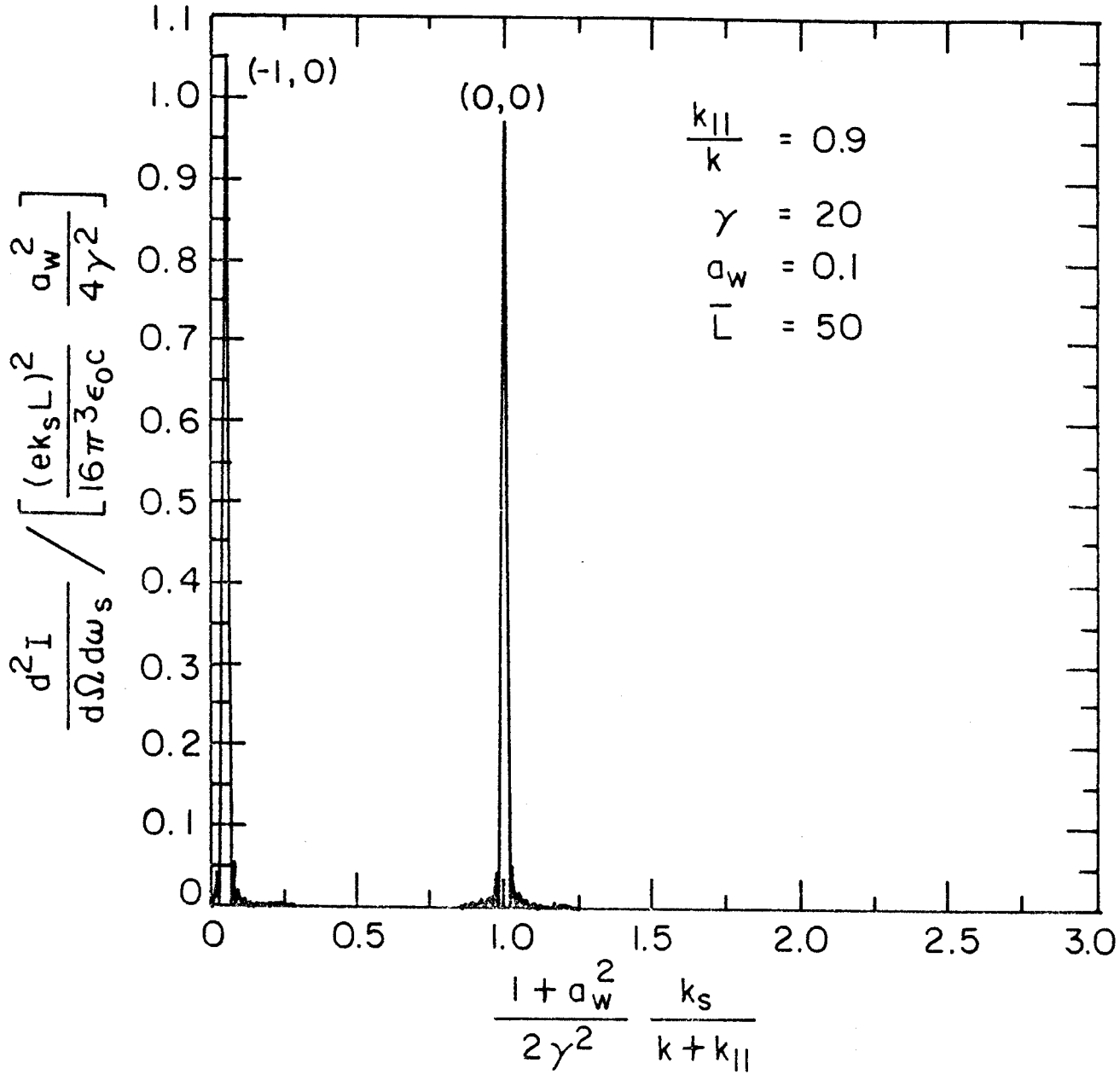
(-1,0)
(0,0)
$\frac{k_{||}}{k} = 0.9$
$\gamma = 20$
$a_w = 0.1$
$\bar{L} = 50$
$\frac{d^2I}{d\Omega d\omega_s} / \left[\frac{(ek_sL)^2}{16\pi^3\epsilon_0 c} \frac{a_w^2}{4\gamma^2}\right]$
$\frac{1+a_w^2}{2\gamma^2} \frac{k_s}{k+k_{||}}$
0
0.1
0.2
0.3
0.4
0.5
0.6
0.7
0.8
0.9
1.0
1.1
0.5
1.0
1.5
2.0
2.5
3.0

Fig. 3

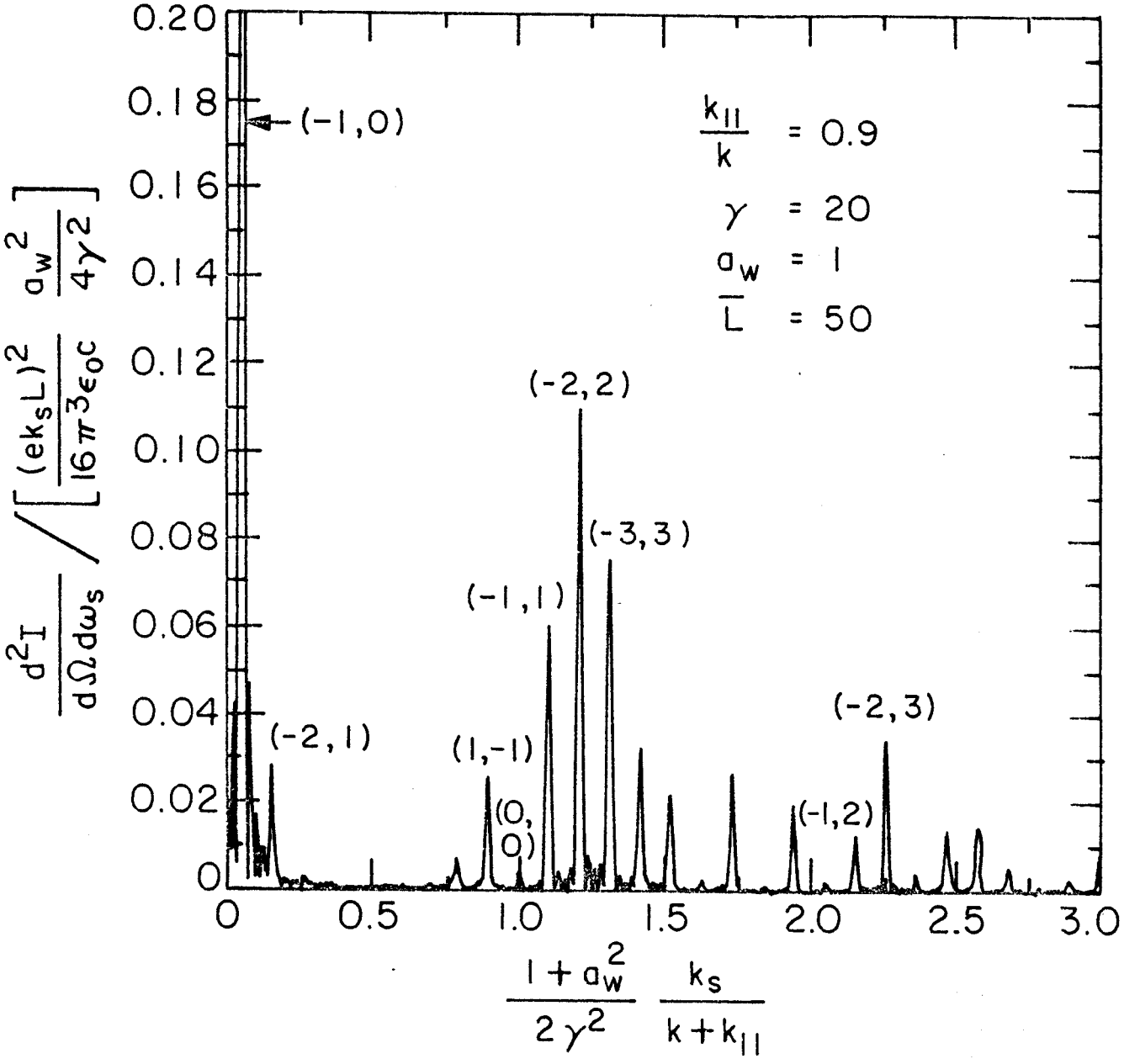
0.20
0.18
0.16
0.14
0.12
0.10
0.08
0.06
0.04
0.02
0
(-1,0)
(-2,1)
(1,-1)
(0, 0)
(-1,1)
(-2,2)
(-3,3)
(-1,2)
(-2,3)
$\frac{k_{11}}{k} = 0.9$
$\gamma = 20$
$a_w = 1$
$\overline{L} = 50$
$\frac{d^2I}{d\Omega d\omega_s} \Big/ \left[\frac{(ek_sL)^2}{16\pi^3\epsilon_0 c}\frac{a_w^2}{4\gamma^2}\right]$
0
0.5
1.0
1.5
2.0
2.5
3.0
$\frac{1+a_w^2}{2\gamma^2}\frac{k_s}{k+k_{11}}$

Fig. 4

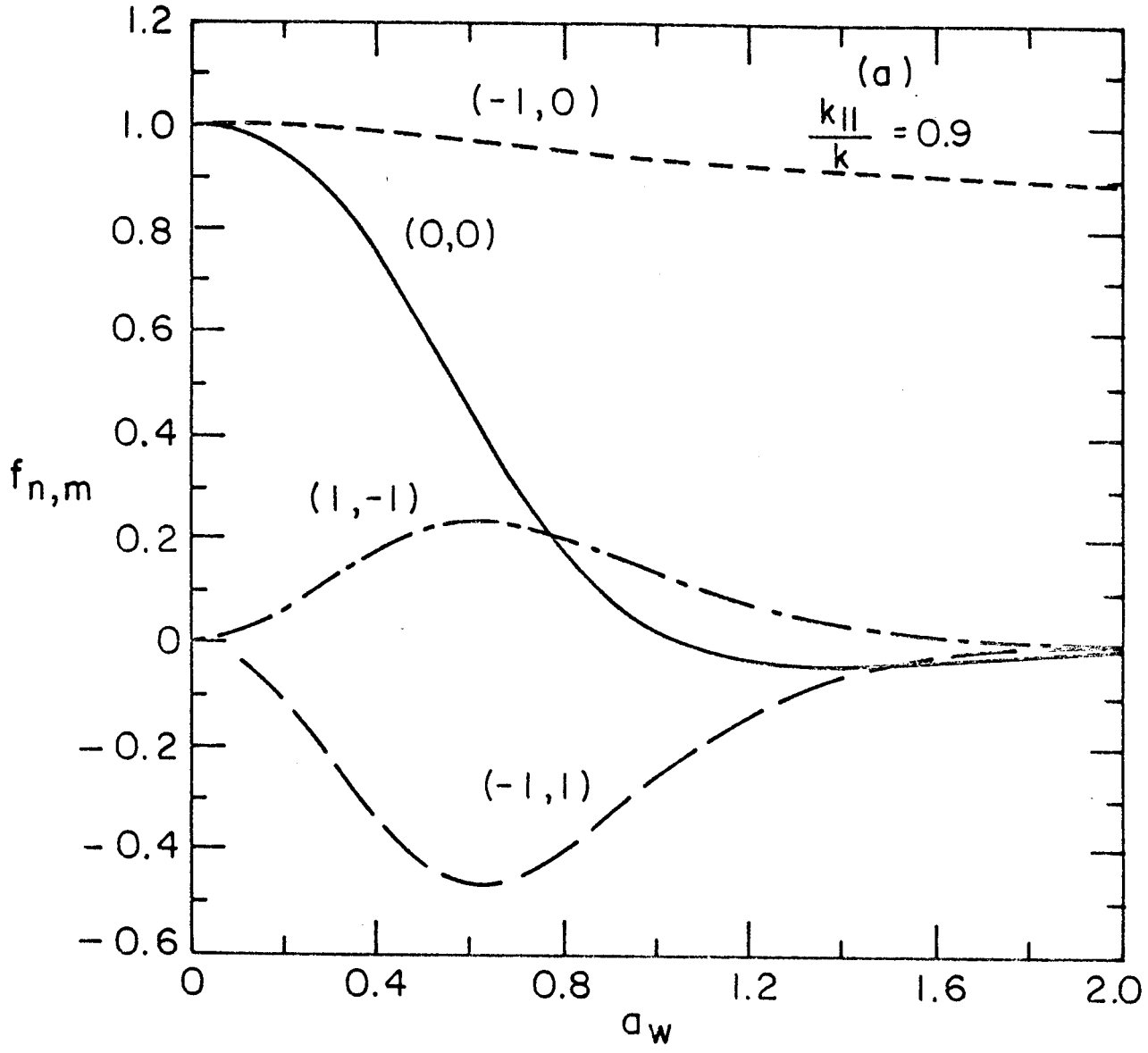
1.2
1.0
0.8
0.6
0.4
0.2
0
-0.2
-0.4
-0.6
0
0.4
0.8
1.2
1.6
2.0
$f_{n,m}$
a_w
(a)
$\frac{k_{||}}{k} = 0.9$
(-1,0)
(0,0)
(1,-1)
(-1,1)

Fig. 5a

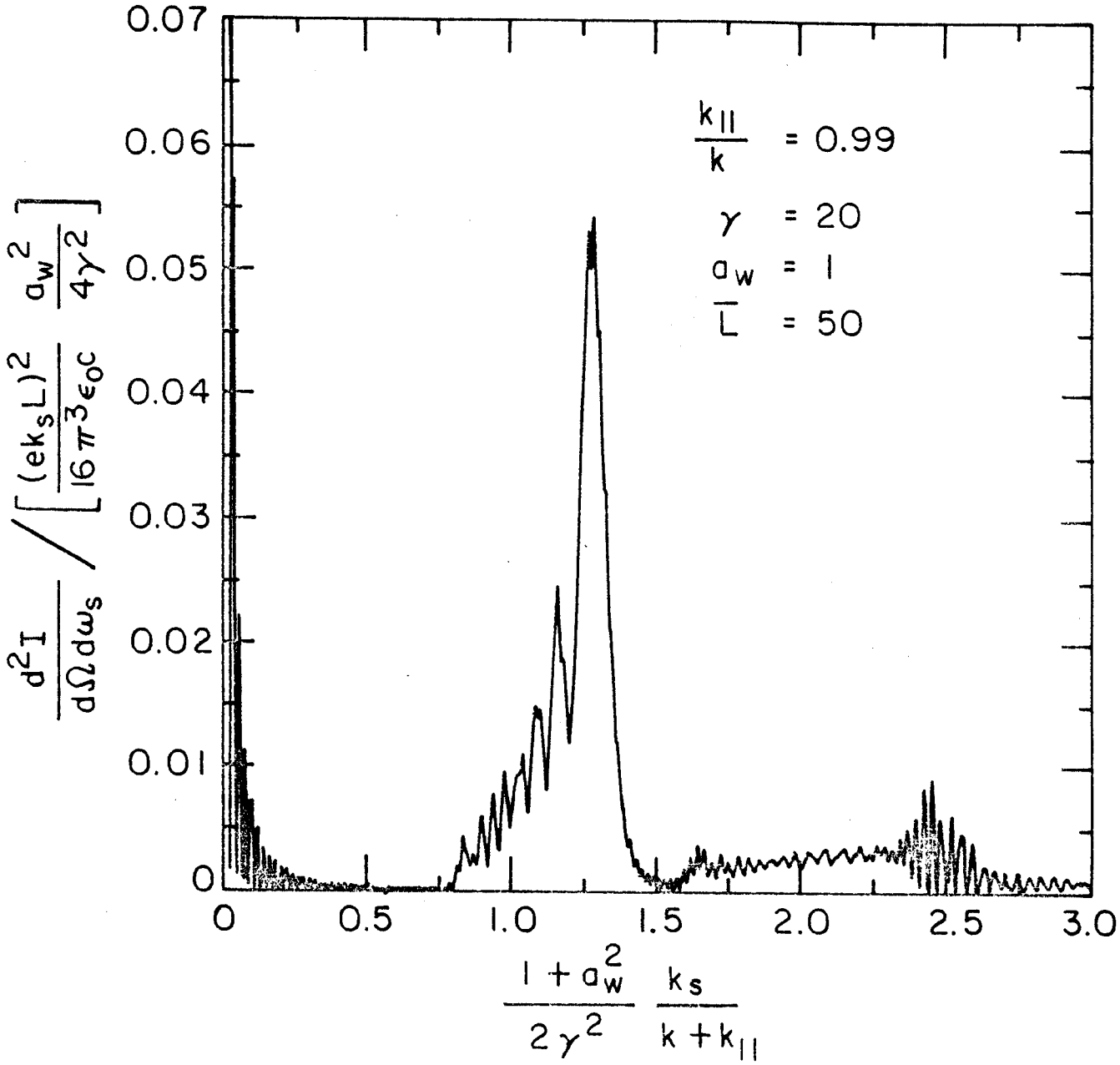
0.07
0.06
0.05
0.04
0.03
0.02
0.01
0
0
0.5
1.0
1.5
2.0
2.5
3.0
$\frac{k_{||}}{k} = 0.99$
$\gamma = 20$
$a_w = 1$
$\bar{L} = 50$
$\frac{d^2I}{d\Omega d\omega_s} \Big/ \left[\frac{(ek_sL)^2}{16\pi^3\epsilon_0 c}\frac{a_w^2}{4\gamma^2}\right]$
$\frac{1+a_w^2}{2\gamma^2}\frac{k_s}{k+k_{||}}$

Fig. 6

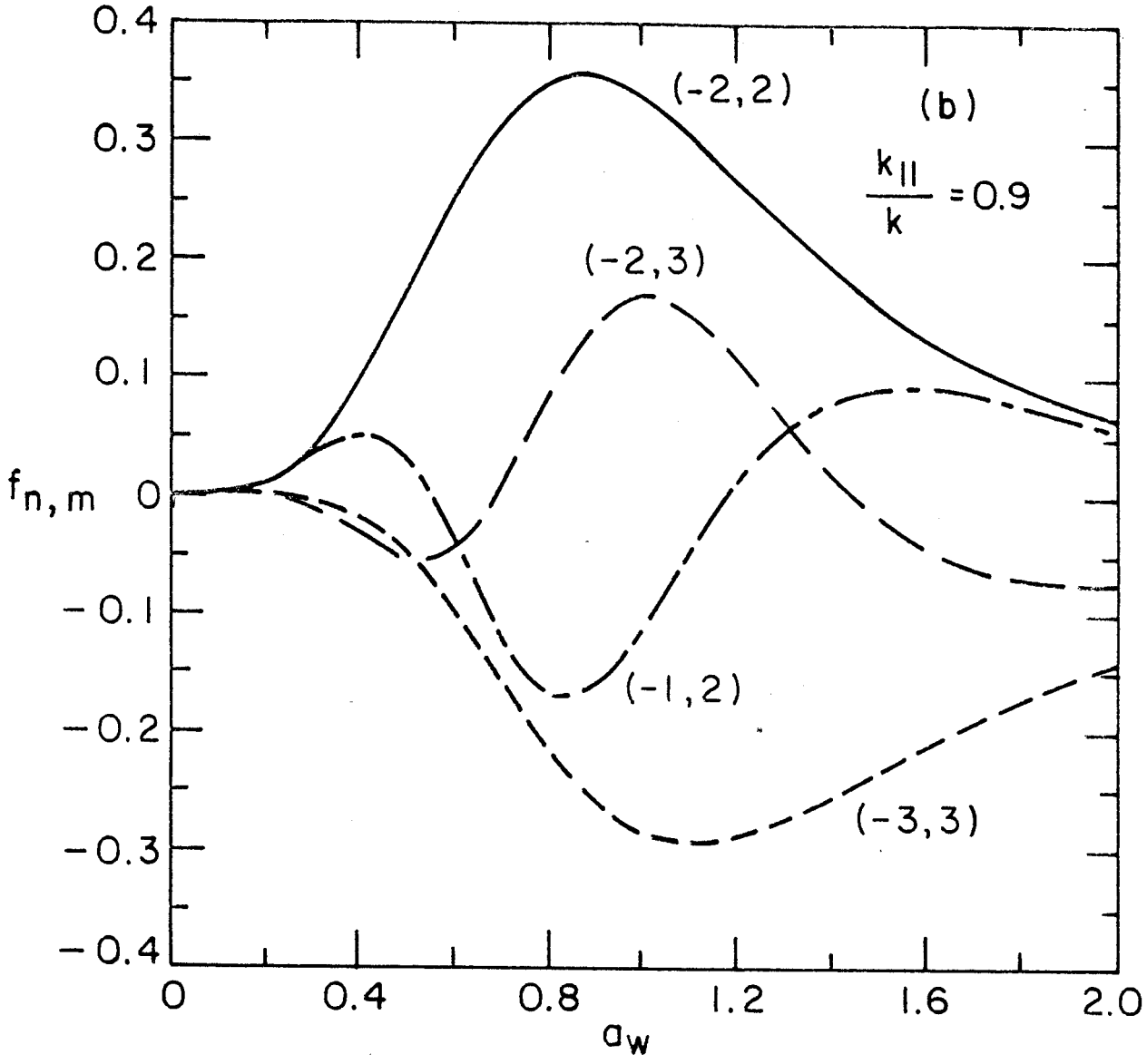
0.4
0.3
0.2
0.1
0
-0.1
-0.2
-0.3
-0.4
$f_{n,m}$
0
0.4
0.8
1.2
1.6
2.0
a_w
(-2,2)
(b)
$\frac{k_{||}}{k} = 0.9$
(-2,3)
(-1,2)
(-3,3)

Fig. 5b